Electrode engineering considerations for high energy efficiency Li-CO_2 batteries

Jingzhao Wang, Xin Chen, Xiangming Cui, Mi Zhou, Jianan Wang, Wenbiao Liu, Hang Ma, Jose Anguita, S. Ravi P. Silva, Kai Yang*, Wei Yan*

J. Z. Wang, X. Chen, X. M. Cui, M. Zhou, Dr. J. N. Wang, Prof. W. Yan.

a. Department of Environmental Science and Engineering, State Key Laboratory of Multiphase Flow in Power Engineering, School of Energy and Power Engineering, Xi'an Jiaotong University, Xi'an 710049, China.

E-mail: wangjn116@xjtu.edu.cn

Dr J. Anguita, Prof. *S. R. P. Silva,* Dr. K. Yang

b. Advanced Technology Institute, University of Surrey, Guildford, Surrey GU2 7XH, UK.

E-mail: kai.yang@surrey.ac.uk

W. B. Liu, Dr. H. Ma

c. Center of Research & Development, Yunnan Yuntianhua Co., LTD, 1417 Dianchi Road, Kunming 650228, China

Materials

Chloroplatinic acid hexahydrate ($H_2PtCl_6·6H_2O$) was obtained from Macklin. Few-layer graphene oxide powder (JCFRGO) and multi-walled carbon nanotube film (JCMWCFM 10μm) were purchased from Jiacai Technology Co., Ltd. Single-walled carbon nanotubes suspension (TNWDIS, 0.2 wt.%) was purchased from Chengdu Organic Chemicals Co. Ltd. Polyacrylonitrile (PAN, average Mw = 150000) and N,N-dimethylformamide (DMF) was obtained from Sigma-Aldrich.

Figure S1. The photograph of hydrogel after hydrothermal treatment.

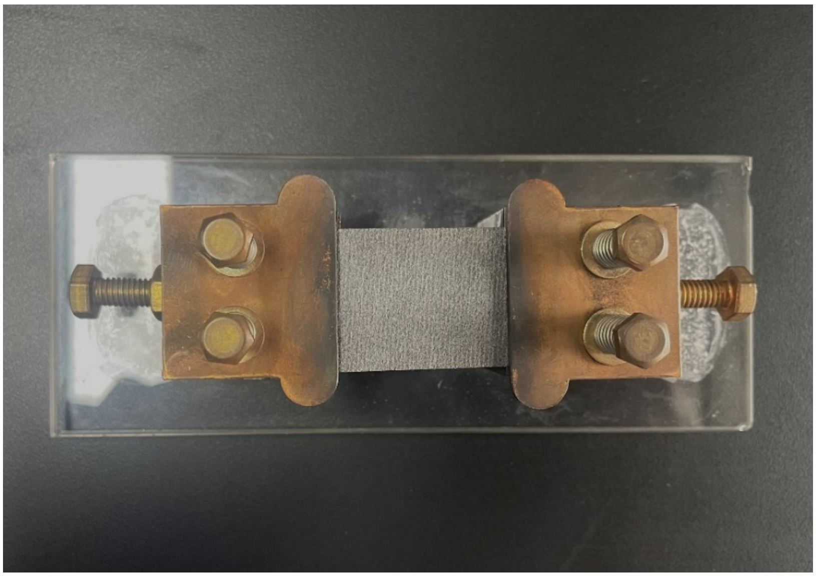

Figure S2. The photograph of the sample holder for Joule heating system.

Table S1. Comparation of key parameters for various substrate materials.

Substrates	**Conductivity**	**Electrolyte wettability**	**Porous structure**	**Specific surface area**	**Mechanical strength**	**Preparation Difficulty**
GCA	Relatively High	Good	Hierarchical porosity	Large	Relatively Strong	Low
CNT	High	Relatively Good	Single porosity	Relatively large	Strong	High
PAN-based CNF	Relatively Low	Relatively Good	Single porosity	Relatively small	Relatively weak	Relatively High

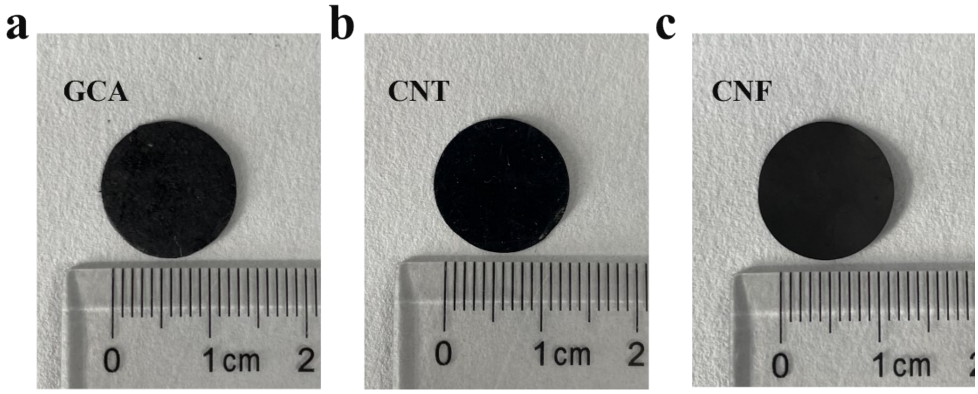

Figure S3. The photograph of the three substrates, the dimeter of the electrode is 14 mm.

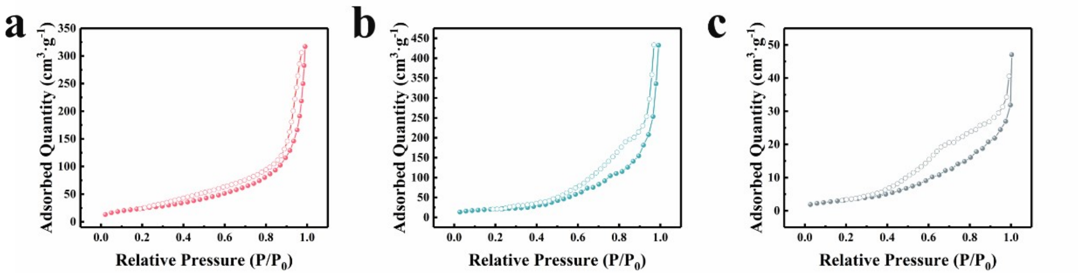

Figure S4. N_2 adsorption-desorption isotherms of (a) GCA, (b) CNT and (c) CNF.

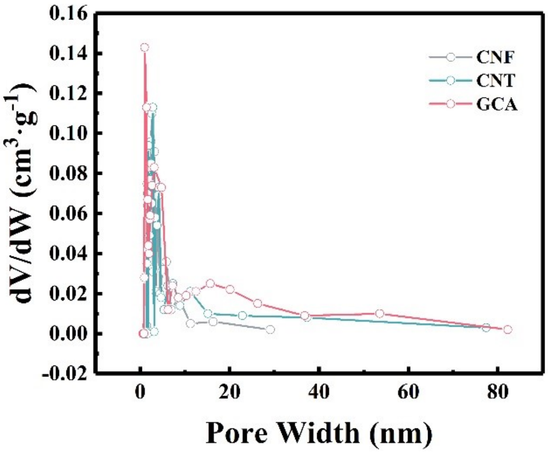

Figure S5. The pore distributions of three substrates based on Barrett–Joyner–Halenda method.

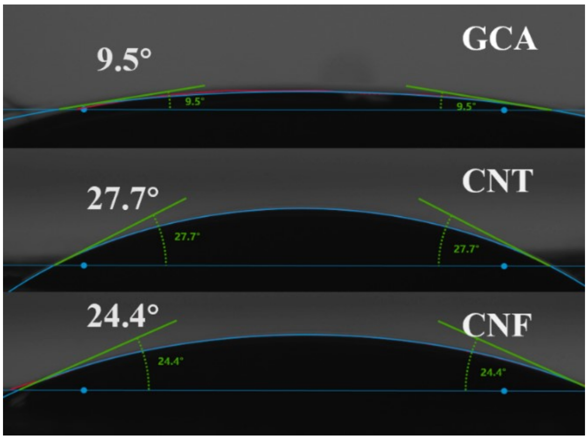

Figure S6. The contact angle test images of three substrates

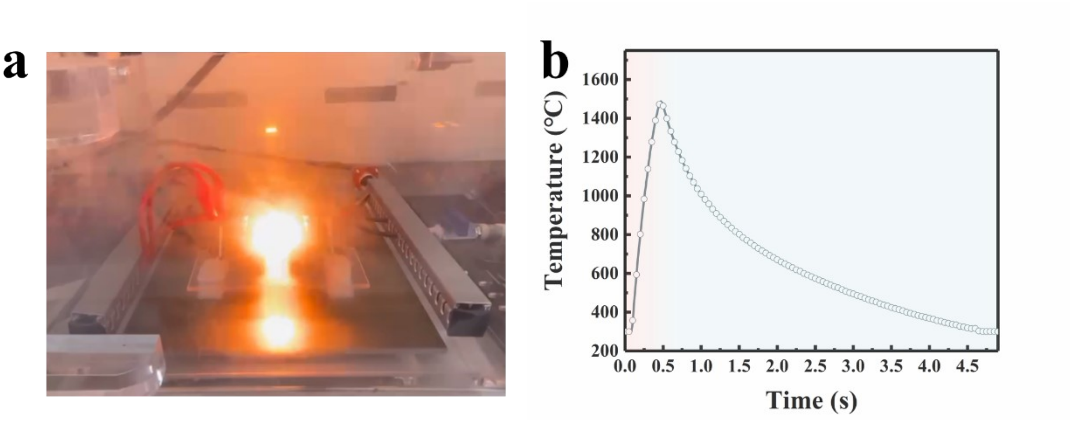

Figure S7. (a) The digital image and (b) the temperature-time curve during Joule-heating process.

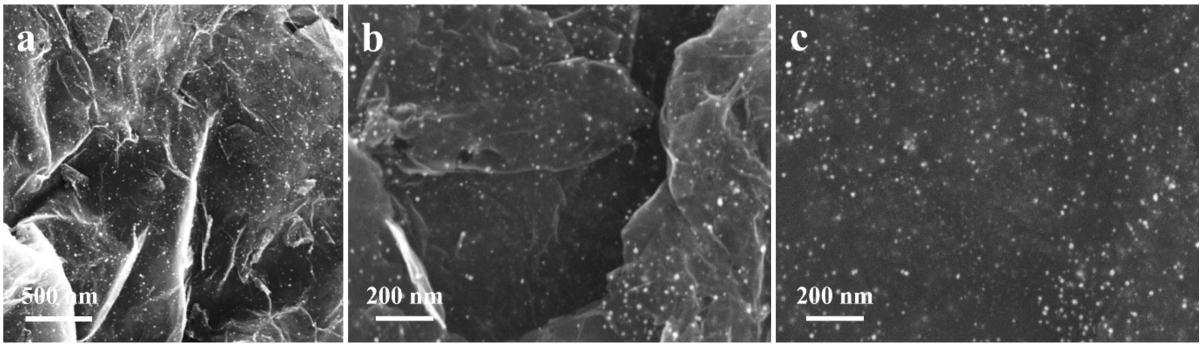

Figure S8. The SEM image of Pt@GCA in (a) and (b) InLens and (c) SE2 modes.

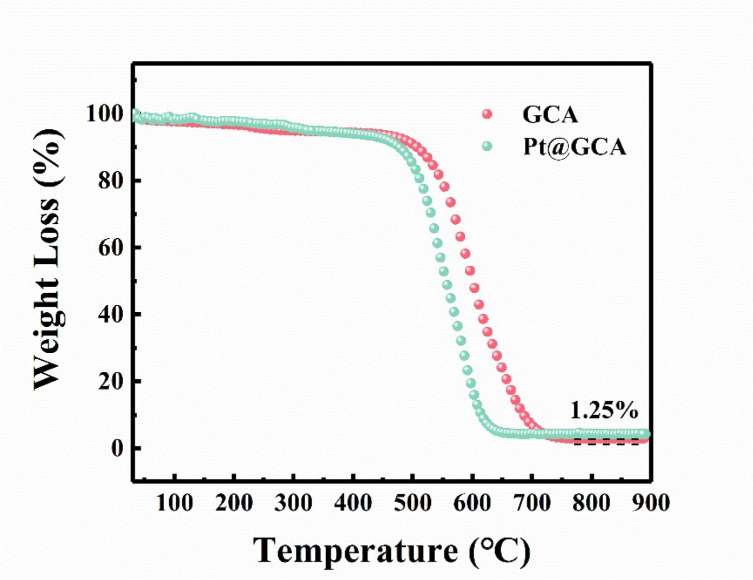

Figure S9. Thermogravimetry curves of GCA and Pt@GCA.

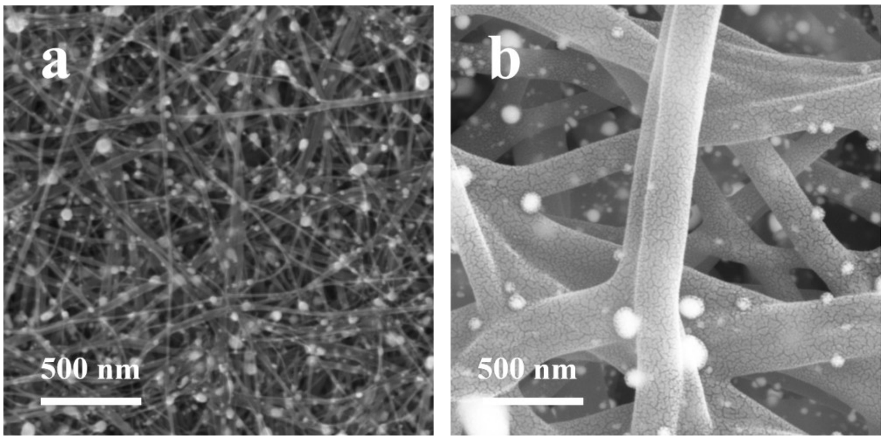

Figure S10. SEM images of (a) Pt@CNT and Pt@CNF electrodes.

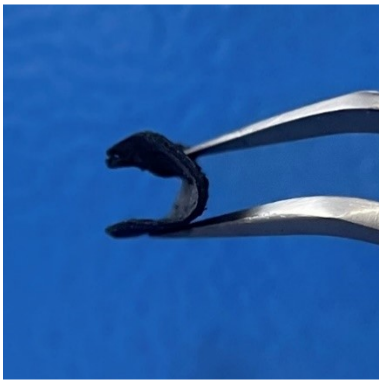

Figure S11. Flexibility test image of Pt@GCA electrode.

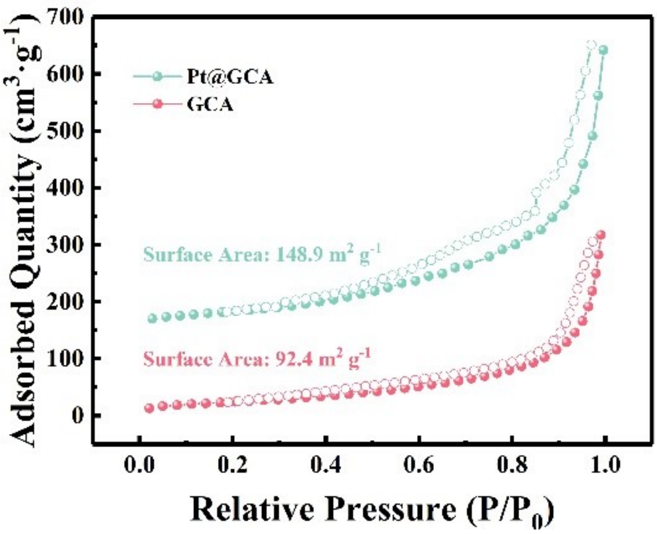

Figure S12. N_2 adsorption-desorption isotherms of Pt@GCA and GCA electrodes.

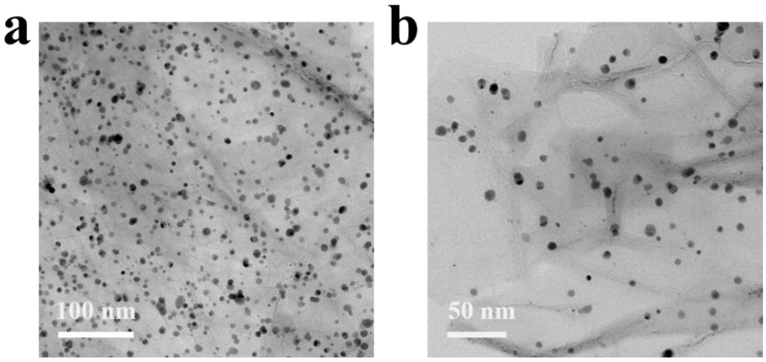

Figure S13. The TEM images of the Pt@GCA cathode with different resolutions.

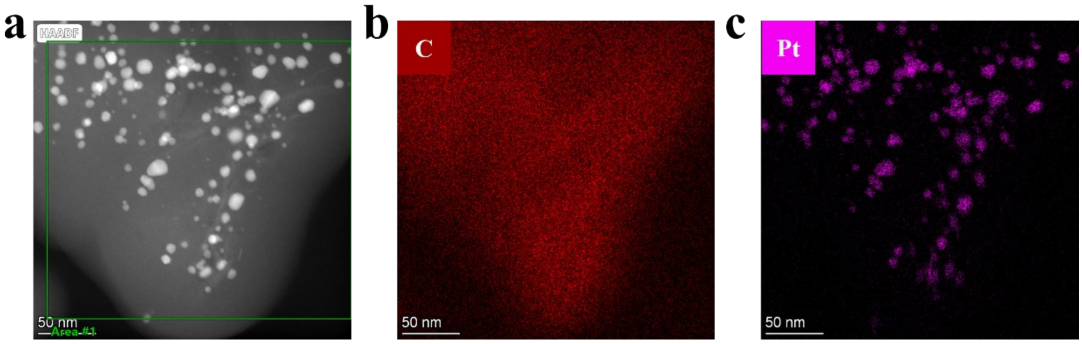

Figure S14. EDS element mappings of Pt@GCA.

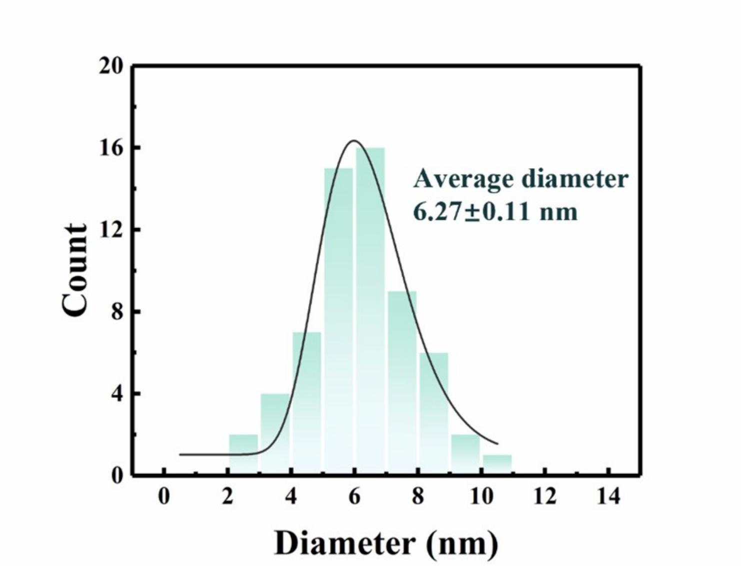

Figure S15. Pt NPs size distribution analysis based on **Figure S13b**.

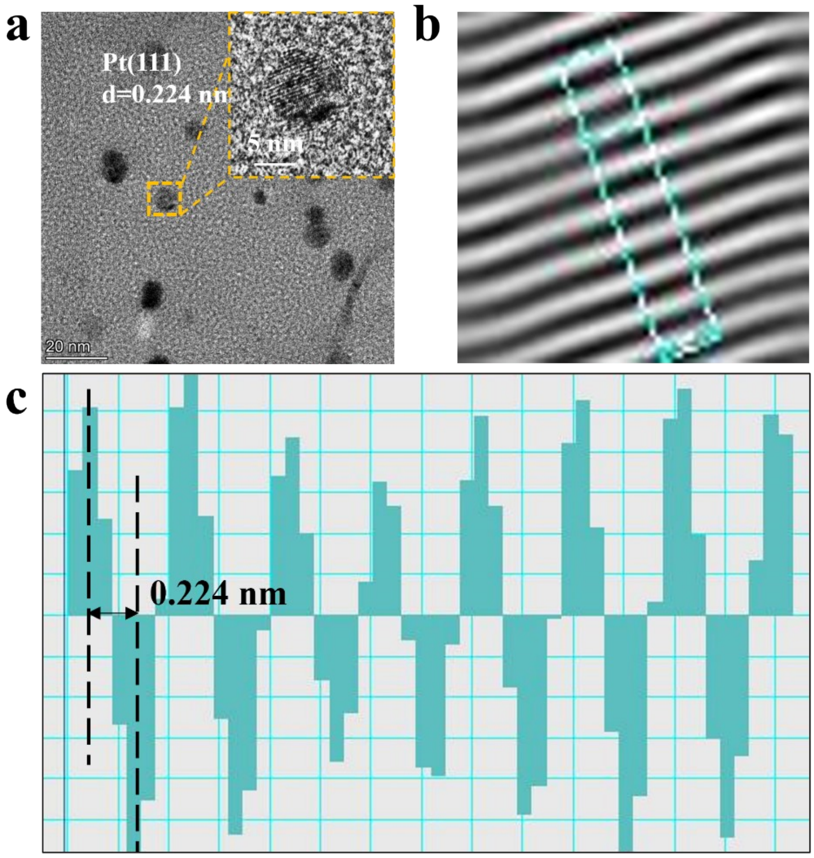

Figure S16. (a) The HRTEM images of the Pt@GCA, (b) the fast Fourier transform (FFT) image and (c) corresponding lattice size.

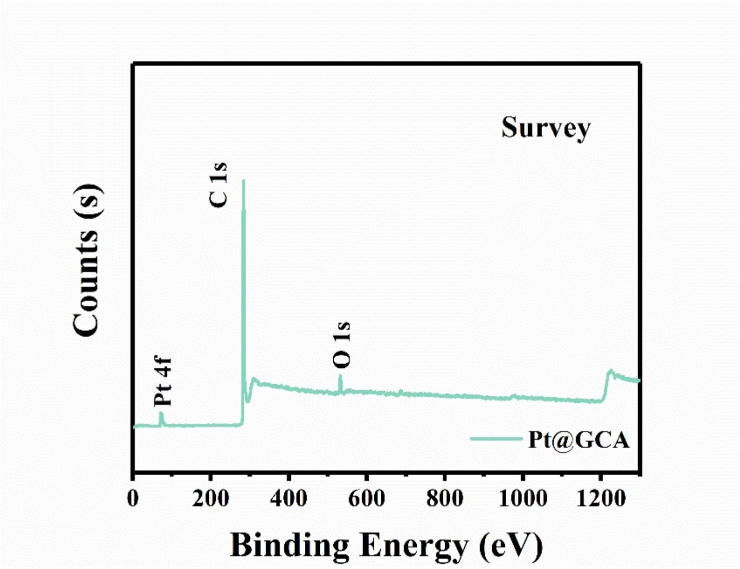

Figure S17. XPS survey of Pt@GCA electrode.

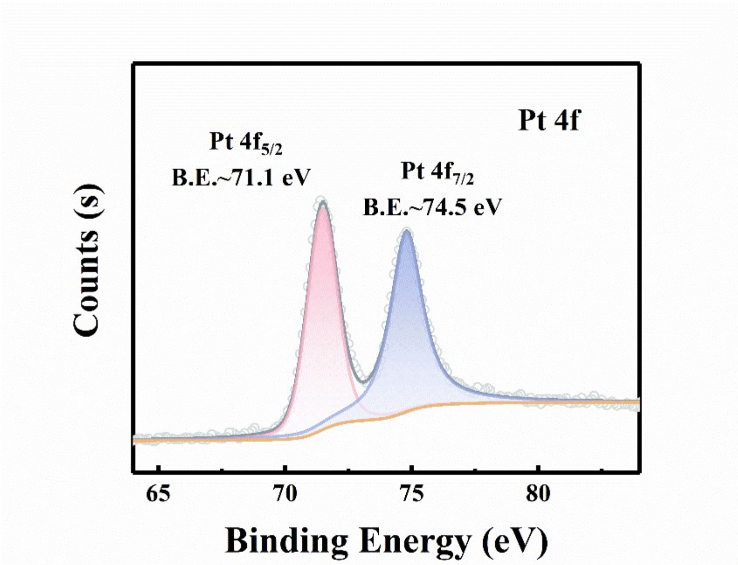

Figure S18. Refined Pt 4f XPS spectrum of Pt@GCA.

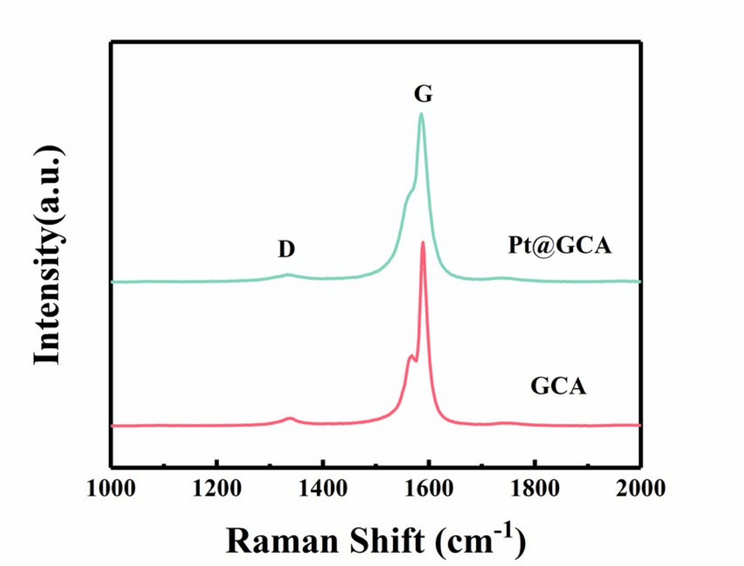

Figure S19. Raman spectra of GCA and Pt@GCA electrodes.

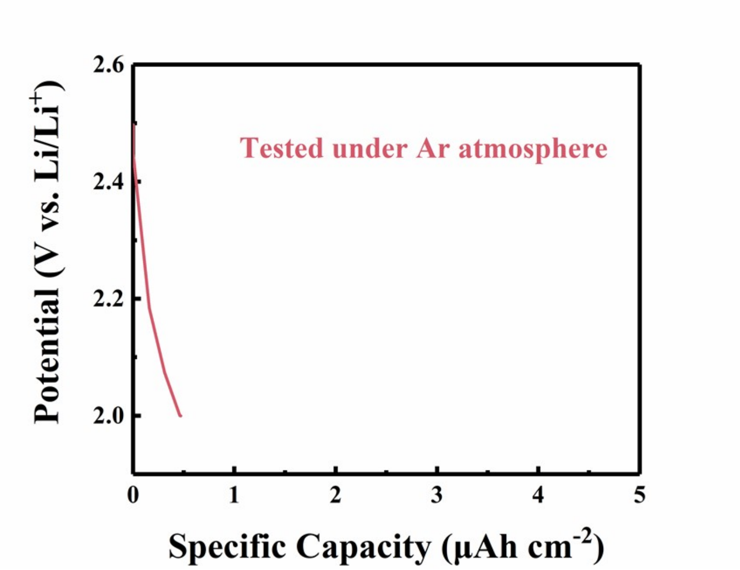

Figure S20. Full discharging test of Pt@GCA under Ar atmosphere, the current density is 20 μA cm^{-2}.

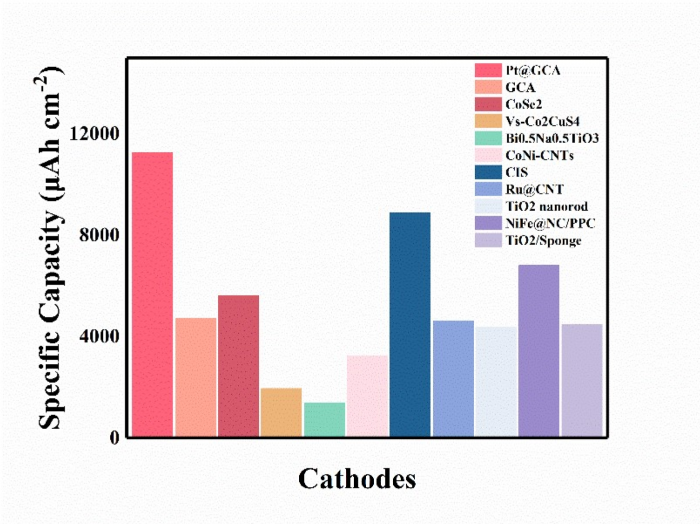

Figure S21. Areal discharging capacity comparison of different cathodes with reported LCBs.

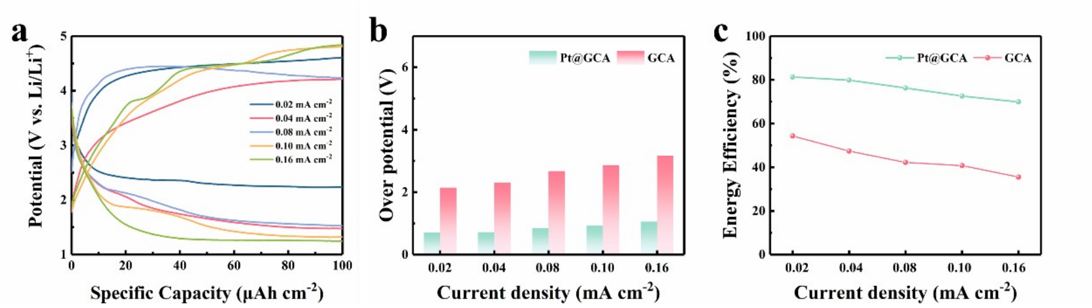

Figure S22. (a) Rate performance of GCA cathodes. (b) Overpotential and (c) energy efficiency of Pt@GCA and GCA under different current densities.

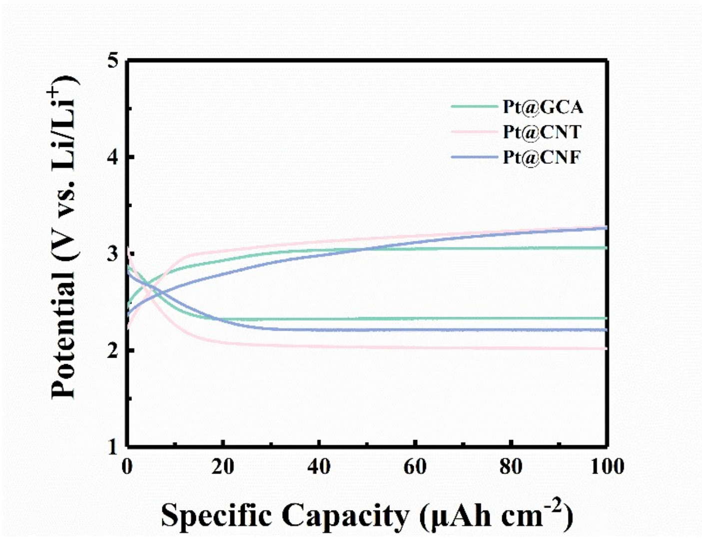

Figure S23. The discharge-charge profiles comparation of LCBs.

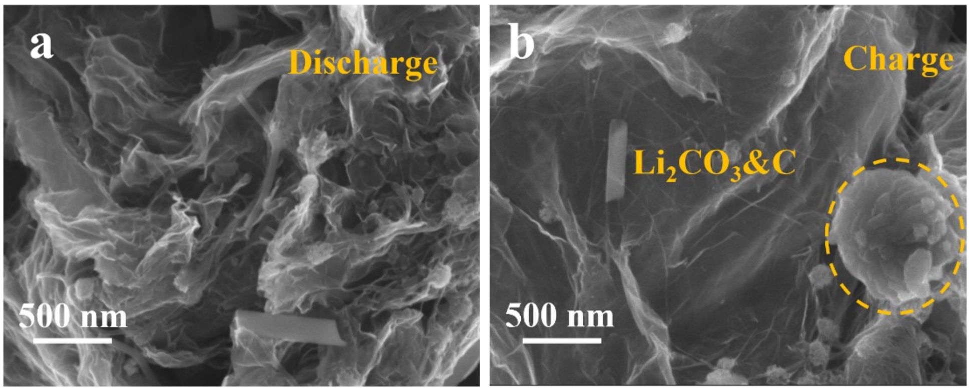

Figure S24. SEM observation of GCA cathode after discharging and charging process.

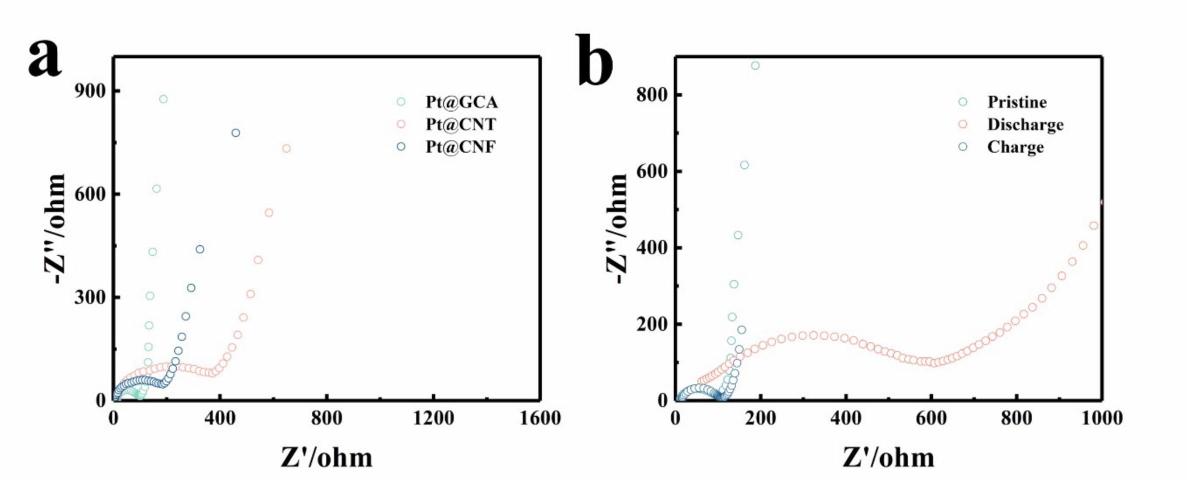

Figure S25. (a) EIS test of different cathodes before cycling. (b) Pt@GCA based LCBs at different cycling state.

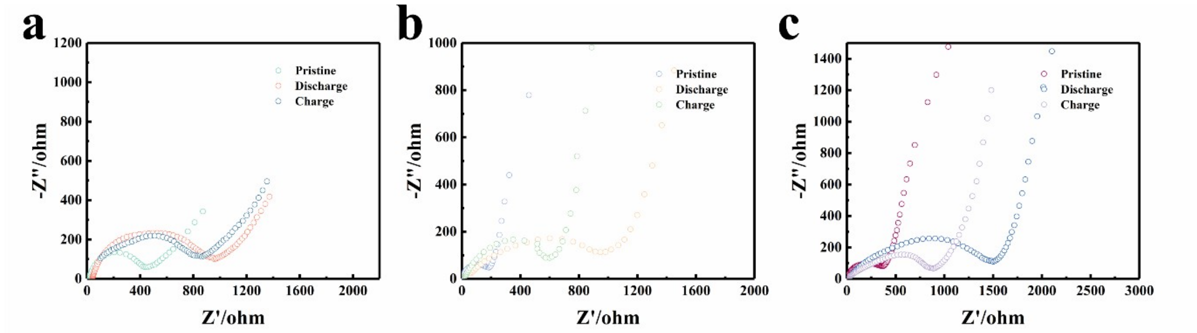

Figure S26. EIS test of (a) GCA, (b) Pt@CNF and (c) Pt@CNT after discharge/charge.

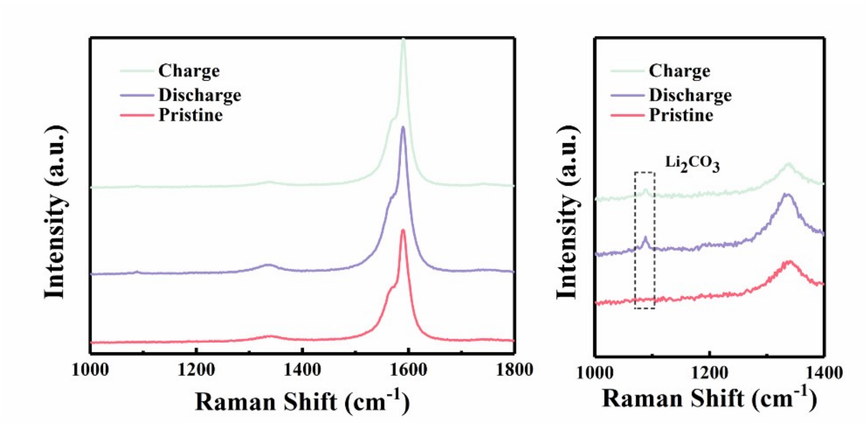

Figure S27. Raman spectra of GCA at different stages.

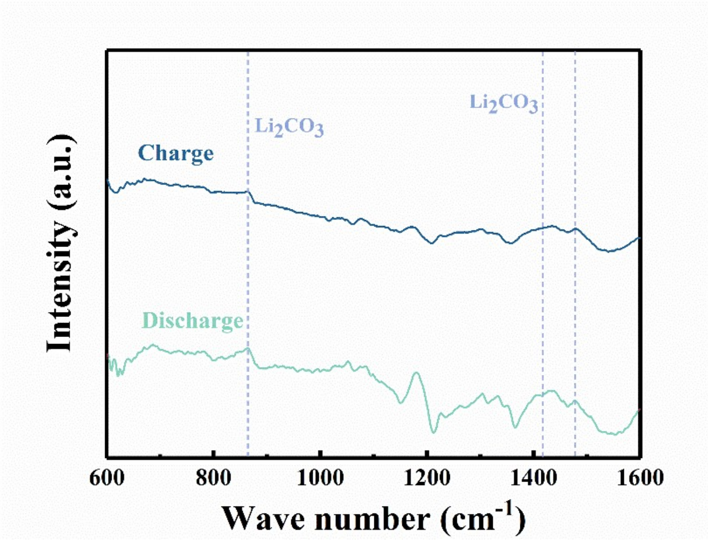

Figure S28. FTIR observation of Pt@GCA cathode after discharging and charging process.

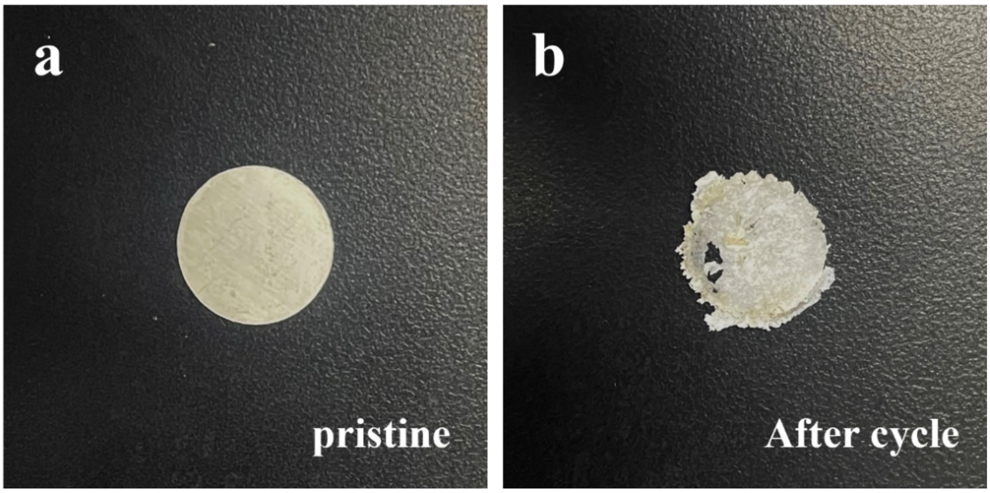

Figure S29. The optical photograph of Li foil (a) before cycling and (b) after operated in LCBs for 800 h.

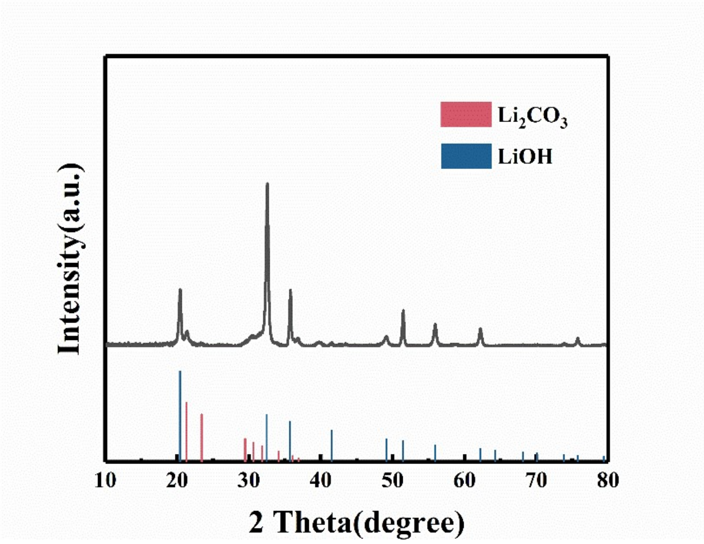

Figure S30. XRD spectra of Li foil after 800 h cycle.

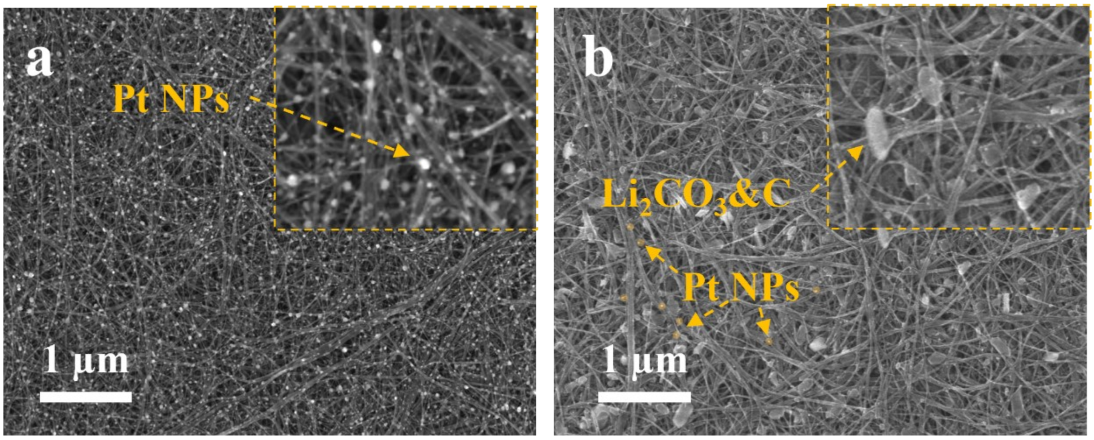

Figure S31. The SEM images of Pt@CNT electrode (a) before and (b) after discharge

Table S2. Electrochemical performance comparison of different reported Li-CO_2 batteries.

Cathodes	Overpotential	Energy efficiency	Discharge capacity	Stability	Ref
Pt@GCA	0.72 V at 20 μA cm^{-2}	82% at 20 μA cm^{-2}	10.03 mAh cm^{-2} at 20 μA cm^{-2}	> 91 cycles at 40 μA cm^{-2}	**This Work**
GCA	2.15 V at 20 μA cm^{-2}	53.15% at 20 μA cm^{-2}	4.72 mAh cm^{-2} at 20 μA cm^{-2}	45 cycles at 20 μA cm^{-2}	**This Work**
Defect-rich porous carbon (c-p-MOF-5)	1.25 V at 0.1 A g^{-1}	N/A	22000 mAh g^{-1} at 0.5 A g^{-1}	540 h at 0.5 A g^{-1}	1
Ru/NS-G	1.40 V at 0.02 mA cm^{-2}	N/A	2.49 mAh cm^{-2} at 20 μA cm^{-2}	100 cycles at 100 mA g^{-1}	2
$CoSe_2$ carbonized melamine foam	0.72 V at 0.05 mA cm^{-2}	81.5% at 0.05 mA cm^{-2}	5.62 mAh cm^{-2} at 0.05 mA cm^{-2}	162 cycles at 20 μA cm^{-2}	3
NiFe@NC/PPC	1.08 V at 0.05 mA cm^{-2}	N/A	6.80 mAh cm^{-2} at 0.05 mA cm^{-2}	109 cycles at 0.05 mA cm^{-2}	4
Vs-Co_2CuS_4	0.73 V at 20 μA cm^{-2}	80.3% at 20 μA cm^{-2}	1.95 mAh cm^{-2} at 20 μA cm^{-2}	600 h at 20 μA cm^{-2}	5
$Bi_{0.5}Na_{0.5}TiO_3$ nanorods piezoelectric	1.00 V at 0.01 mA cm^{-2}	N/A	1.37 mAh cm^{-2} at 0.01 mA cm^{-2}	100 h at 0.01 mA cm^{-2}	6
Porous carbon C/CoNi-CNTs	1.47 V at 0.05 mA cm^{-2}	N/A	3.24 mAh cm^{-2} at 0.05 mA cm^{-2}	100 cycles at 0.05 mA cm^{-2}	7
Copper indiμm sμlfide (CIS)	1.00 V at 20 μA cm^{-2}	~80% at 20 μA cm^{-2}	8.88 mAh cm^{-2} at 20 μA cm^{-2}	105 cycles at 20 μA cm^{-2}	8
TiVC/graphene aerogel	1.50 V at 200 mA g^{-1}	~65% at 200 mA g^{-1}	27 880 mAh g^{-1} at 100 mA g^{-1}	91 cycles at 100 mA g^{-1}	9
N, O-doped graphene aerogel	1.00 V at 20 μA cm^{-2}	78.46% at 20 μA cm^{-2}	18.69 mAh cm^{-2} at 20 μA cm^{-2}	151 cycles at 20 μA cm^{-2}	10
Co-doped CeO_2/graphene aerogel	1.25 V at 100 mA g^{-1}	N/A	7860 mAh g^{-1} at 100 mA g^{-1}	100 cycles at 100 mA g^{-1}	11

NiS_2/FeS_2-N, S, Co-doped graphene aerogel	1.10 V at 100 mA g^{-1}	71.50% at 200 mA g^{-1}	21178 mAh g^{-1} at 300 mA g^{-1}	127 cycles at 100 mA g^{-1}	12
Pt/N-doped polypyrrole CNT	0.75 V at 100 mA g^{-1}	N/A	29614 mAh g^{-1} at 100 mA g^{-1}	30 cycles at 100 mA g^{-1}	13
Pt@CNT	1.86 V at 100 mA g^{-1}	70 % at 100 mA g^{-1}	N/A	110 cycles at 100 mA g^{-1}	14
Ru@CNT	1.39 V at 20 µA cm^{-2}	N/A	4.62 mAh cm^{-2} at 20 µA cm^{-2}	100 cycles at 20 µA cm^{-2}	15
TiO_2 nanorod arrays/ sponge	1.02 V at 0.05 mA cm^{-2}	N/A	4.38 mAh cm^{-2} at 0.05 mA cm^{-2}	1600 h at 0.05 mA cm^{-2}	16

Reference

1. J. Han, H. Wu, R. Song, W. Mao, D. Wang and D. Liu, *Electrochim. Acta*, 2024, **477**, 143779.
2. Y. Qiao, J. Wu, J. Zhao, Q. Li, P. Zhang, C. Hao, X. Liu, S. Yang and Y. Liu, *Energy Storage Mater.*, 2020, **27**, 133-139.
3. K. Wang, L. Liu, D. Liu, Y. Wei, Y. Liu, X. Wang, A. S. Vasenko, M. Li, S. Ding, C. Xiao and H. Pan, *Small*, 2024, **20**, e2310530.
4. H. Liang, Y. Zhang, F. Chen, S. Jing, S. Yin and P. Tsiakaras, *Appl. Catal., B*, 2019, **244**, 559-567.
5. B. Lu, B. Chen, D. Wang, C. Li, R. Gao, Y. Liu, R. Mao, J. Yang and G. Zhou, *Proc. Natl. Acad. Sci.*, 2023, **120**, e2216933120.
6. S. L. Tian, M. L. Li, L. M. Chang, W. Q. Liu and J. J. Xu, *J Colloid Interface Sci*, 2024, **656**, 146-154.
7. X. Ji, Y. Liu, Z. Zhang, J. Cui, Y. Fan and Y. Qiao, *J Colloid Interface Sci*, 2024, **655**, 693-698.
8. L. Chen, J. Zhou, J. Zhang, G. Qi, B. Wang and J. Cheng, *Energy Environ. Mater.*, 2023, **6**, e12415.
9. W. Zhao, Y. Yang, Q. Deng, Q. Dai, Z. Fang, X. Fu, W. Yan, L. Wu and Y. Zhou, *Adv.Funct.Mater.*, 2022, **33**, 2210037.
10. W. Yu, L. Liu, Y. Yang, N. Li, Y. Chen, X. Yin, J. Niu, J. Wang and S. Ding, *Chem. Eng. J.*, 2023, **465**, 142787.
11. Q. Deng, Y. Yang, S. Qu, W. Wang, Y. Zhang, X. Ma, W. Yan and Y. Zhang, *Energy Storage Mater.*, 2021, **42**, 484-492.
12. Y. Jin, Y. Liu, L. Song, J. Yu, K. Li, M. Zhang and J. Wang, *Chem. Eng. J.*, 2022, **430**, 133029.
13. Z. Chen, M. Yuan, Z. Tang, H. Zhu and G. Zeng, *Phys Chem Chem Phys*, 2023, **25**, 7662-7668.
14. P.-F. Zhang, T. Sheng, Y. Zhou, Y.-J. Wu, C.-C. Xiang, J.-X. Lin, Y.-Y. Li, J.-T. Li, L. Huang and S.-G. Sun, *Chem. Eng. J.*, 2022, **448**, 137541.
15. S. Thoka, C. M. Tsai, Z. Tong, A. Jena, F. M. Wang, C. C. Hsu, H. Chang, S. F. Hu and R. S. Liu, *ACS. Appl. Mater. Interfaces.*, 2021, **13**, 480-490.
16. X.-X. Wang, G.-J. Ji, P. She, F. Li, Q.-C. Liu, H.-F. Wang and J.-J. Xu, *Chem. Eng. J.*, 2021, **426**, 131101.